Calculation of Structural, Electronic, Optical, and Thermoelectric Properties of XPdBi (X = La, Sc, Y): Materials for Optoelectronic Devices

O. Addou, A. Touia* and K. Benyahia

Materials Science and Applications Laboratory, Faculty of Sciences and Technology, University of Ain Temouchent, Belhadj Bouchaib. BP 284, Ain-Temouchent, 46000, Algeria

Received: 03.01.2023 & Accepted: 18.01.2023

Doi: 10.12693/APhysPolA.143.252 *e-mail: amina.touia@univ-temouchent.edu.dz

The structural, electronic, optical, and thermoelectric properties of half-Heusler LaPdBi, ScPdBi, and YPdBi alloys were investigated using the full-potential linearized augmented plane wave based on density functional theory and implemented in the WIEN2K code. To properly describe the electronic structures and, subsequently, the optical and thermoelectric properties, we chose the generalized gradient approximation parameterized by the Perdew–Burke–Ernzerhof functional and performed the modified Becke–Johnson correction method, which described all the electronic, optical, and thermoelectric parameters with high accuracy for these three selected compounds. The transport behavior of these materials indicates that they are potential candidates for thermoelectric applications. The optical and thermoelectric properties presented in this study were obtained using the modified Becke–Johnson method and generalized gradient approximation. These alloys, XPdBi (X = La, Sc, Y), have almost the same characteristics as the optical quantities, and the prediction of optical properties shows that studied compounds are ideal materials for optoelectronic applications, renewable energies, and solar cells. Our results are in good agreement with those reported in the literature.

topics: XPdBi (X = La, Sc, Y), electronic, FP-LAPW, optoelectronic, thermoelectric

1. Introduction

In this study, we are particularly interested in half-Heusler XPdBi (X = La, Sc, Y). The main objective is to develop new semiconductors suitable for optoelectronic applications, such as thin film solar cells or laser diodes [1]. To achieve this objective, a detailed study of the electronic structure and optical and thermoelectric properties of XPdBi (X = La, Sc, Y) was performed. Technological advancements in various fields of physics depend on the development of new materials and techniques for their processing. These techniques for calculating the electronic structure have been developed over the last decades, in particular, the *ab-initio* methods, which have now become a basic tool for the calculation of the physical properties of the most complex systems. They are also a tool of choice for the prediction of new materials and have sometimes been able to replace experiments that are very expensive or even impossible to carry out in the laboratory. Among these *ab-initio* methods, the full potential linearized augmented plane wave (FP-LAPW) method [2] is currently one of the most precise methods for calculating the electronic structure of solids within the framework of density functional theory (DFT) [3]. Thus, the computational speed of the FP-LAPW method is impressive compared with the other first-principle methods. It is enough to know the composition of the materials to be able to simulate them from the resolution of the equations of quantum mechanics. We performed relativistic scalar calculations of the structural, electronic, optical, and thermoelectric properties of XYZ half-Heusler, using the Wien2k code [4]. Researchers are interested in XPdBi (X = Y, Sc, La) because of its thermoelectric properties [5]. The narrow energy gap and sharp peaks in the density of states around the Fermi level result in the high thermoelectric power of these compounds. According to Cook et al. [5, 6], the compound LaPdBi exhibits this important property. Hai-Jun Zhang et al. [7] reported that the semi-conductive behavior of these compounds results from their strong tendency for covalent bonding and that they are closed-shell, nonmagnetic, and semi-conductive species, as discovered in half-Heusler rare-earth compounds XYBi (e.g., YPdBi, LuPdBi, GdPtBi, ScPtBi, and ScNiBi). Many theoretical studies have indicated that the indirect band gap semiconductor ScPdBi exhibits *sp* band inversion under conditions such as high pressure or when Sc is replaced with other elements (e.g., Lu, Y, or Gd) [8]. These XPdBi (X = La, Sc, Y) of the formula XYZ crystallize

TABLE I

Lattice constant a_0 (in [Å]), bulk modulus B (in [GPa]), its pressure derivative B' and minimum energy at equilibrium E_0 (in [Ry]) using GGA-PBE.

	a_0 [Å]	B [GPa]	B'	E_0 [Ry]
		LaPdBi		
GGA-PBE (present work)	6.9664	70.6252	4.1556	−70252.766505
Exper.	6.825 [16], 6.859 [17], 6.8708 [18]	–	–	–
Theor.	6.98 [5], 6.843 [19], 6.825 [19, 20]	72.25 [5], 77.83 [19]	4.43 [5]	–
		ScPdBi		
GGA-PBE (present work)	6.5359	81.4931	5.4109	−54785.860465
Exper.	6.449 [21], 6.52 [22], 6.56 [23], 6.788 [24], 6.432 [17]	–	–	–
Theor.	6.5752 [8], 6.57 [25], 6.529 [26], 6.365 [24]	84.81 [26]	–	–
		YPdBi		
GGA-PBE (present work)	6.7685	63.0912	5.5200	−60028.863643
Exper.	6.64 [5, 8, 16, 19–27]	–	–	–
Theor.	6.570 [24]	–	–	–

in a non-centrosymmetric cubic structure (space group number 216, F-43m, $C1b$) [9], which can be derived from the tetrahedral structure of ZnS type by filling in the lattice octahedral sites; this type of half-Heusler structure can be characterized by the interpenetration of three face-centered cubic (fcc) sub lattices, each of which is occupied by atoms X, Y, and Z [9, 10]. The positions occupied are 4a (1/2, 1/2, 1/2), 4b (1/4, 1/4, 1/4), and 4c (0, 0, 0). The crystal structure of XPdBi (X = La, Sc, or Y) is shown in Fig. 1. These materials XPdBi (X = La, Sc, Y) are highly efficient in conducting heat and are perfectly applicable as thermoelectric materials [11]. In our work, we conducted a comparative study of the structural, electronic, optical, and thermoelectric properties of half-Heusler materials based only on bismuth (Bi). This comparative study is not available, either experimentally or theoretically. Therefore, this was a detailed predictive study.

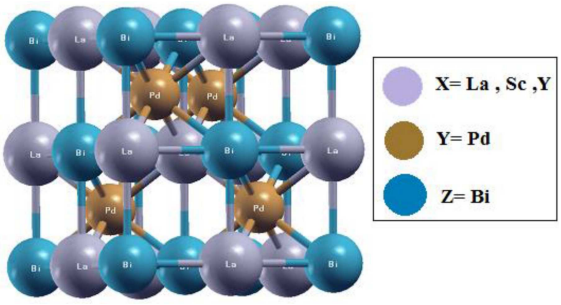

Fig. 1. Crystal structure of XPdBi (X = La, Sc, Y).

2. Computational method

In the present work, we studied the physical properties of XPdBi (X = La, Sc, Y) alloys using FP-LAPW based on DFT and implemented in the WIEN2K code [2–4]. To treat the exchange and correlation energies, we used the generalized gradient approximation of Perdew–Burke–Ernzerhof (GGA-PBE) [12]. The approximation developed by Becke and Johnson (mBJ) modified by Tran and Blaha (TB-mBJ) [13] was also applied. This approach is designed to improve the values of the energy gaps. In this study, we also expanded the basic functions up to $R_{MT}\,K_{\max} = 10$, where R_{MT} is the smallest muffin radius in the unit cell, and $K_{\max}$ is the plane wave radius. The radial expansion of potential and charge density is performed up to $l_{\max} = 10$. The R_{MT} radii were chosen to be as wide as possible to avoid overlapping of the spheres; thus, for the three compounds LaPdBi, ScPdBi, and YPdBi, R_{MT} was set at 2.5 a.u for the La, Sc, Y, Pd, and Bi atoms. For the integration in the reciprocal space of k, we have found that a $14 \times 14 \times 14$ k-point grid is sufficient to ensure the convergence of the total energy and the charge density, which is equivalent to 104 special k-points in the Brillouin irreducible zone [14]. In all calculations, a self-consistent cycle was reached with an energy convergence of 10^{-4} eV.

3. Results and discussion

3.1. Structural properties

The determination of equilibrium structures is a fundamental step in any calculation. The total energy was calculated by varying the volume to determine the equilibrium lattice parameter and bulk modulus, and the curves were fitted by the Murnaghan equation of state [15].

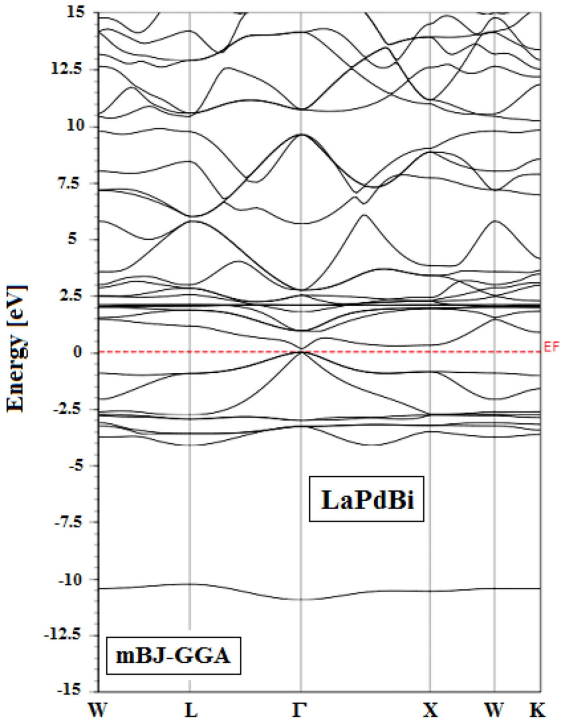

Fig. 2. The band structure of LaPdBi at the equilibrium structure using mBJ-GGA approximation.

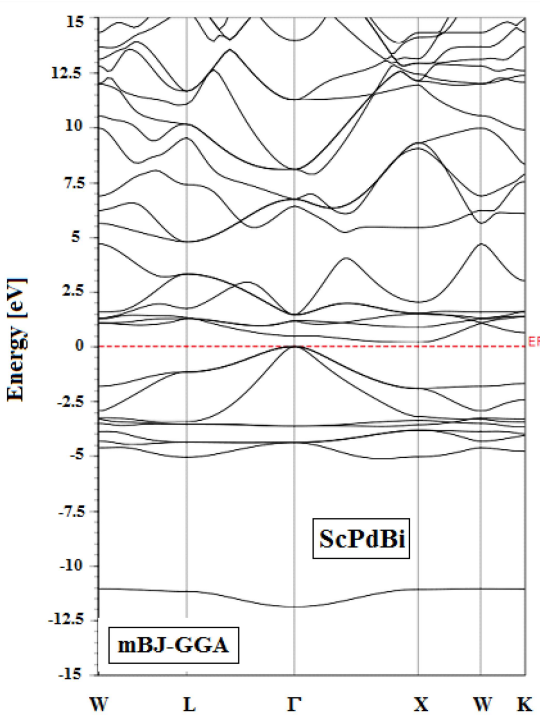

Fig. 3. The band structure of ScPdBi at the equilibrium structure using mBJ-GGA approximation.

The structural parameters results (lattice constants (a) and bulk modulus (B), its pressure derivative (B'), and minimum energy at equilibrium E_0) are listed in Table I [5, 8, 16–27]. The calculated lattice constants and the bulk moduli of the XPdBi (X = La, Sc, Y) semiconductors are in good agreement with the experimental and theoretical results [5, 8, 16, 19–25]. The calculated lattice constants of XYZ systems differ only slightly from their experimental analogs [16, 21–24].

3.2. Electronic properties

In this section, we discuss the electronic structures of the half-Heusler alloys LaPdBi, ScPdBi, and YPdBi. Figures 2–4 show the band structures along the high symmetry points of the Brillouin zone calculated using the modified Becke–Johnson method and generalized gradient approximation (mBJ-GGA). We notice through these results that the two compounds ScPdBi and YPdBi have indirect gaps in the direction Γ–X. However, for LaPdBi, the most important remark is the presence of a direct gap in the valence band and the conduction band at the Γ point. The mBJ-GGA approximation, which is best suited to calculating the gap, gives values of the order of 0.452, 0.191, and 0.19 eV for the three compounds LaPdBi, ScPdBi, and YPdBi, respectively. The electronic parameter results are listed in Table II [5, 18–20, 28]. Our results are in good agreement with experimental

TABLE II

The calculated values of band gap of XPdBi (X = La, Sc, Y) at $T = 0$ K and $P = 0$ GPa.

	LaPdBi Gap [eV] at Γ	ScPdBi Gap [eV] at Γ–X	YPdBi Gap [eV] at Γ–X
mBJ-GGA	0.452	0.191	0.19
GGA-PBE	0.147	0.021	0.18
Exper.	0.05 [28] 0.053 [18]	–	–
Theor. GGA-PBE	0.315 [5] 0.23 [19] 0.31 [20]	–	–

and theoretical ones. Direct gap materials and indirect gap materials behave very differently from an optoelectronic point of view because the charge carriers of the direct gap materials can move from one band to another by simply exchanging a photon, whose momentum is negligible at these energy levels, while the carriers of the indirect gap materials must interact with both a photon and a phonon to modify their wave vector, which makes the transition much less probable.

The partial density of state (PDOS) calculated using the modified Becke-Johnson potential approximation (mBJ-GGA) for compounds XPdBi

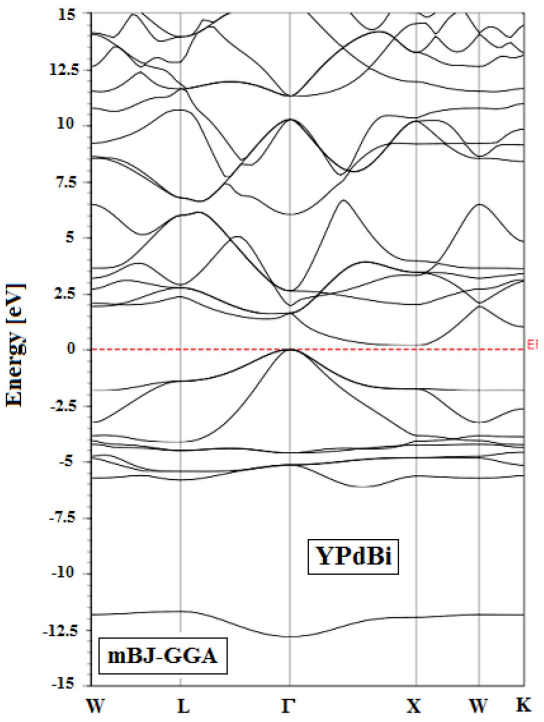

Fig. 4. The band structure of YPdBi at the equilibrium structure using mBJ-GGA approximation.

(X = La, Sc, Y) are shown in Fig. 5. We observe that below the Fermi level, the valence band is strongly dominated by Pd-*d* states with a contribution, however minor, from Bi-*s* states, whereas above the Fermi level, in the conduction band, the PDOS is dominated by the La-*f*, Sc-*d*, and Y-*d* states. The band structures and density of states show that XPdBi (X = La, Sc, Y) compounds are semiconductors. Our results are in good agreement with the values measured experimentally and theoretically [5, 19–20, 24, 26–27, 29]. The semiconductive behavior of these compounds results from their strong tendency for covalent bonding and from the fact that they are closed-shell, nonmagnetic, and semiconductive species. The narrow energy gap and sharp peaks in the density of states around the Fermi level resulted in the high thermoelectric power of these compounds. Narrow-gap semiconductors are semiconducting materials with a band gap smaller than that of silicon, that is, smaller than 1.11 eV. They were used as the thermoelectric detectors. The PBE functional results in the overestimation of the forbidden band. The overestimation of the forbidden band is explained by the absence of excitonic effects, and the value of the deviation approaches the experimental value when the excitonic effects are included. However, special care should be taken with compounds with small band gaps because of the tendency of PBE to overestimate the dielectric constant near the metallic boundary.

3.3. Optical properties

Optical parameters are important for discovering the performance of new slides, especially for applications in optoelectronics (light sources, sensors, and detectors). For this reason, we have calculated the different optical quantities for the XPdBi (X = La, Sc, Y) alloys, such as the dielectric function (real and imaginary parts), the refractive index, the extinction coefficient, the absorption coefficient, the reflectivity, and optical conductivity. The dielectric function depending on the frequency is a real quantity. On the other hand, in the case of a dynamic field, the dielectric function $\varepsilon(\omega)$ is a complex function [3] given by $\varepsilon(\omega) = \varepsilon_1(\omega) + \varepsilon_2(\omega)$, where $\varepsilon_1(\omega)$ and $\varepsilon_2(\omega)$ are the real part and the imaginary part of the dielectric function, respectively. Figure 6 presents the real part of the dielectric function. The first thing that can be extracted from this figure is the static value $\varepsilon_1(0)$ which corresponds to the value of the real part taken at an energy of zero value, where the values of $\varepsilon_1(0)$ for these three compounds LaPdBi, ScPdBi, and YPdBi are of the order of 23.65, 23.67, and 15.88, respectively. We notice important peaks at the energy points of about 1.15, 0.55, and 1.4 eV for the three compounds LaPdBi, ScPdBi, and YPdBi, respectively, followed by a strong decrease until $\varepsilon_1(\omega)$

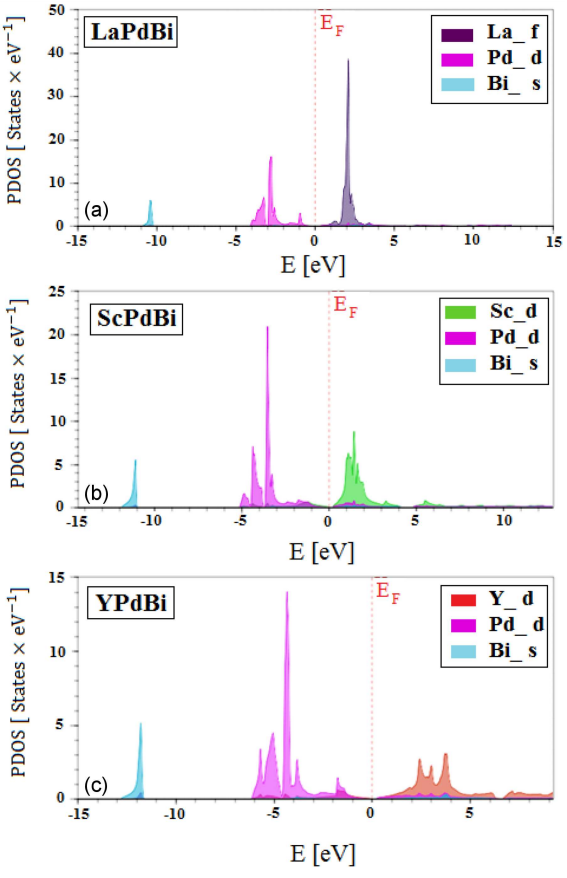

Fig. 5. The partial density of state ofXPdBi (X = La (a), Sc (b), Y (c)) at the equilibrium structure using mBJ-GGA approximation.

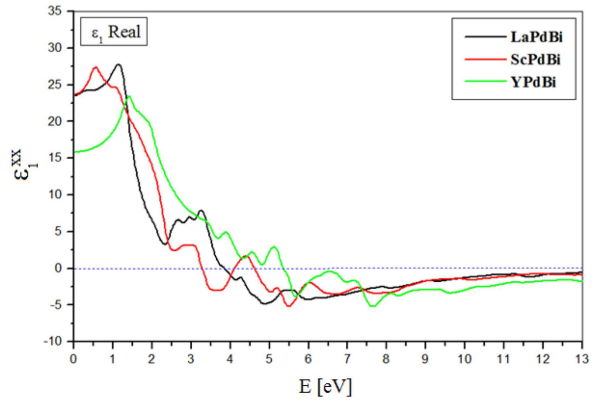

Fig. 6. Real part of dielectric function $\varepsilon_1(\omega)$ of XPdBi (X = La, Sc, Y) compound.

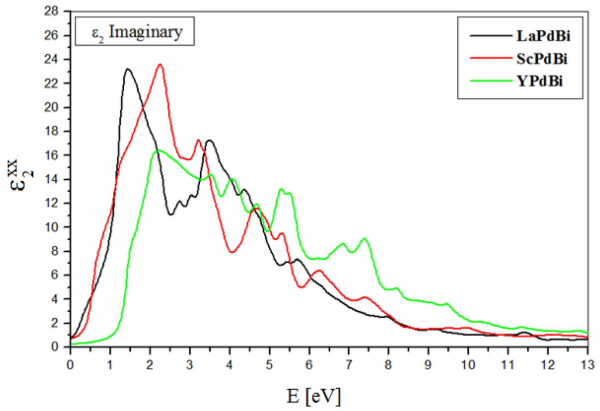

Fig. 7. Imaginer part of dielectric function $\varepsilon_2(\omega)$ of XPdBi (X = La, Sc, Y) compound.

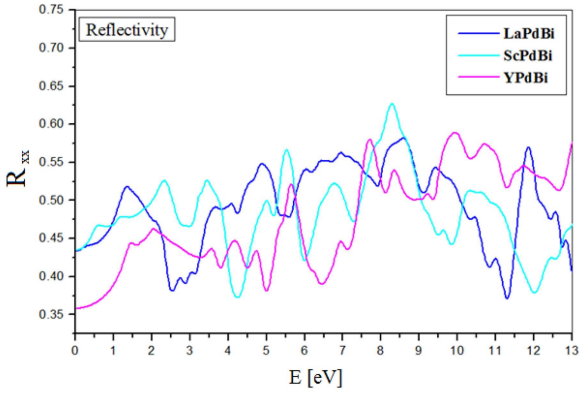

Fig. 8. The reflectivity $R(\omega)$ of XPdZ (X = La, Sc, Y) compounds.

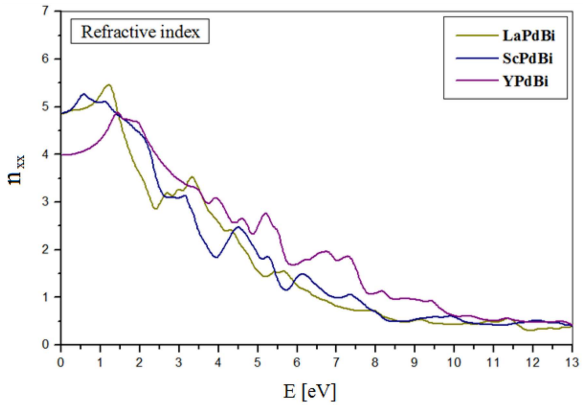

Fig. 9. The refractive index $n(\omega)$ of XPdZ (X = La, Sc, Y) compounds.

becomes negative in the part which starts from the energy values 3.81, 3.27, and 5.35 eV for the three compounds LaPdBi, ScPdBi, and YPdBi, respectively, where this decay is interpreted by the fact that the photons are damped (damping of electromagnetic waves). In the classical case of $\omega_p \gg 1/\tau$, the plasma frequency is the frequency at which the sign of the real part of the dielectric function changes from negative to positive. The analysis of reflection and transmission using Fresnel's equations shows that above the zero crossing, the metal described by the Drude model becomes transparent [30]. The imaginary part of the dielectric function is shown in Fig. 7. We observe in the graph the appearance of the energy gap obtained in the band structure, followed by several peaks distinguished in the energy range between 0 and 8 eV. Using the band structure and the density of state stated in the previous paragraphs, we have identified these different peaks as inter-band transitions, from which we notice peaks of significant height which are located at 1.42, 2.25, and 2.17 eV for the compounds LaPdBi, ScPdBi, and YPdBi respectively. These peaks generally arise from the direct transition of valence electrons to those in the conduction band. Reflectivity is one of the important factors that describe the optical response of solids; it is defined as a ratio of the intensity of the reflected ray to the intensity of the incident ray at the normal incidence of the electromagnetic wave on the system [31]. Figure 8 presents the reflectivity as a function of the photon energy for the half-Heusler XPdBi (X = La, Sc, Y) compounds. In the ultraviolet (UV) region, strong oscillations were observed with very high reflectivities of 58% for the LaPdBi compound, 62% for the ScPdBi compound, and 59% for the YPdBi compound. The refractive index is a very important optical property because it determines the amount of light reflected upon reaching the interface, as well as the critical angle for total internal reflection in optical devices such as photonic crystals, waveguides, and solar cells. The refractive index curves of these XPdBi (X = La, Sc, Y) compounds are shown in Fig. 9. The zero frequency refractive indices $n(0)$ of the LaPdBi, ScPdBi, and YPdBi alloys are 4.88, 4.89, and 4.0, respectively. We notice peaks in the visible region with a strong peak $n = 5.45$, 5.25, and 4.82 for the compounds LaPdBi, ScPdBi,

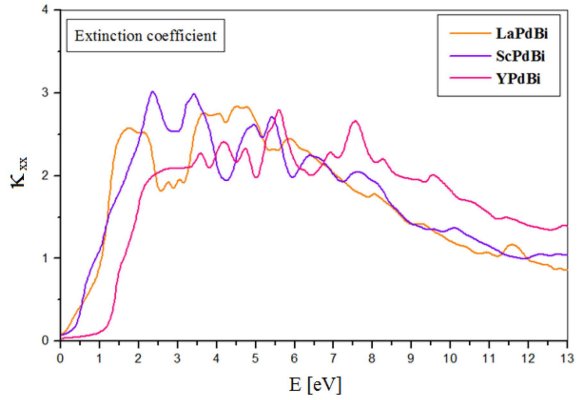

Fig. 10. The extinction coefficient $\kappa(\omega)$ of XPdZ (X = La, Sc, Y) compounds.

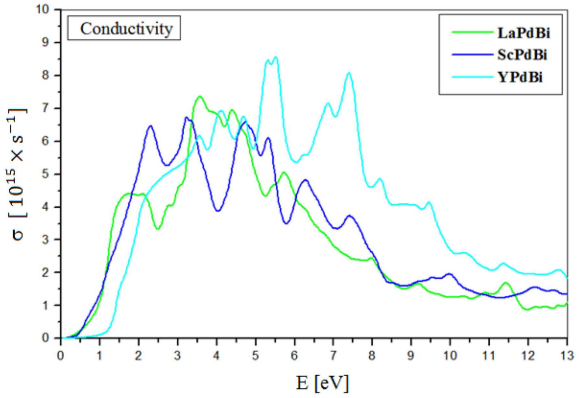

Fig. 11. The conductivity $\sigma(\omega)$ of XPdZ (X = La, Sc, Y) compounds.

and YPdBi, respectively. Figure 10 presents the extinction coefficient as a function of photon energy for the three XPdBi (X = La, Sc, Y) compounds. The zero frequency extinction coefficients $\kappa(0)$ of LaPdBi, ScPdBi, and YPdBi alloys are 0.43, 0.44, and 0.36, respectively. We notice peaks in the UV region with a large peak κ = 0.58, 0.62, and 0.58 for the compounds LaPdBi, ScPdBi, and YPdBi, respectively. The measurable amount of optical reflective substance and the frequency-dependent character are estimated and described accordingly by the optical conductivity factor. The calculated optical conductivities present significant peaks, which are the peaks due to the plasmon frequency, which informs us about the number of electrons that pass from the valence band to the conduction band. We have presented the optical conductivity curves in Fig. 11. The conductivity spectra show significant peaks for the various XPdBi (X = La, Sc, Y) alloys, which are represented in the UV spectrum. The frequency-dependent absorption coefficient is defined as a portion of incident ray energy that is absorbed in a unit length of the crystal. In Fig. 12, one notices a strong absorption in

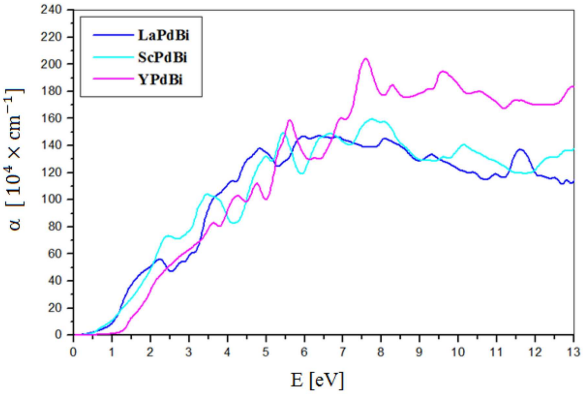

Fig. 12. The absorption of XPdZ (X = La, Sc, Y) compounds.

the UV region for the three compounds LaPdBi, ScPdBi, and YPdBi, with significant peaks of the order of 147.85×10^4 cm^{-1}, 158.32×10^4 cm^{-1}, and 204.26×10^4 cm^{-1}, respectively. For the LaPdBi compound at $T = 0$ K and $P = 0$ GPa, the dielectric function (real and imaginary parts), refractive index, and extinction coefficient are in good agreement with the available theoretical data [19]. For the ScPdBi alloy, the dielectric function (real and imaginary parts), absorption coefficient, reflectivity, refractive index, extinction coefficient, and optical conductivity are in good agreement with available theoretical data [26, 30]. For the YPdBi material, no experimental or theoretical data is available to compare the results obtained for the dielectric function (real and imaginary parts), the absorption coefficient, the reflectivity, the refractive index, the extinction coefficient, and optical conductivity, so it is a detailed predictive study. From the calculation of the optical properties, the results indicate that XPdBi (X = La, Sc, Y) compounds are transparent materials in the infrared (IR) region. Therefore, these materials are suitable candidates for optoelectronic applications under visible light and UV regions.

3.4. Thermoelectric properties

We used the BoltzTraP code [32] to study the thermoelectric behavior of the three chosen compounds XPdBi (X = La, Sc, Y). We show in Fig. 13 the electrical conductivity as a function of the Fermi energy (E_F) at different temperatures (200, 400, 600, and 800 K) for the three compounds XPdBi (X = La, Sc, Y). The three compounds show approximately the same behavior at given temperatures. The value of the electrical conductivity of the three compounds LaPdBi, ScPdBi, and YPdBi decreases progressively until E_F = 0.59 Ry, E_F = 0.564 Ry, and E_F = 0.83 Ry, respectively, then increases beyond these values. Our results show that the maximum electrical conductivity is 2.2486×10^{20} $(\Omega\ m\ s)^{-1}$, 2.0109×10^{20} $(\Omega\ m\ s)^{-1}$,

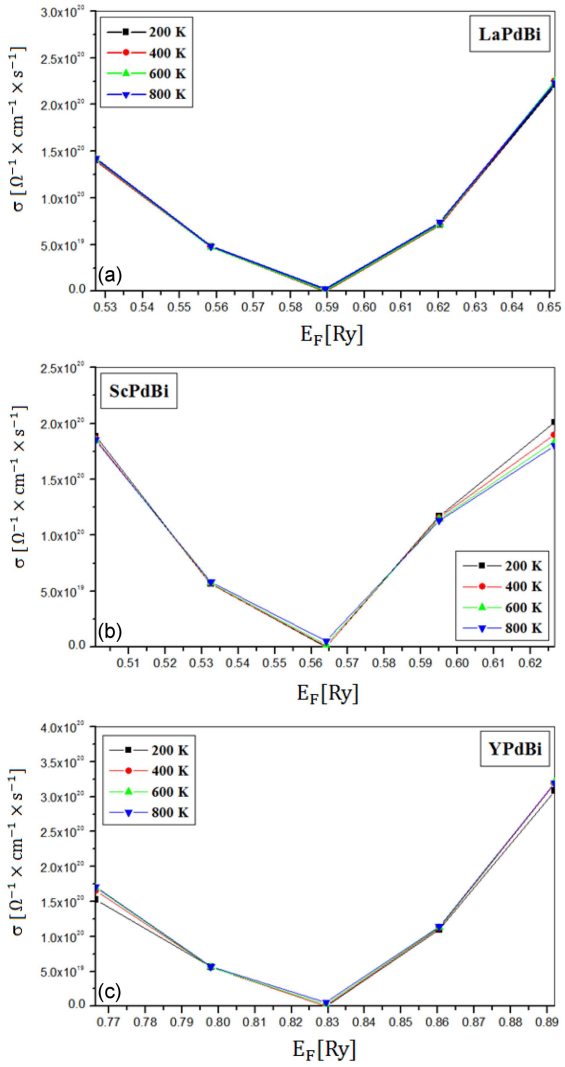

Fig. 13. The variation of the electrical conductivity for XPdBi (X = La (a), Sc (b), Y (c)).

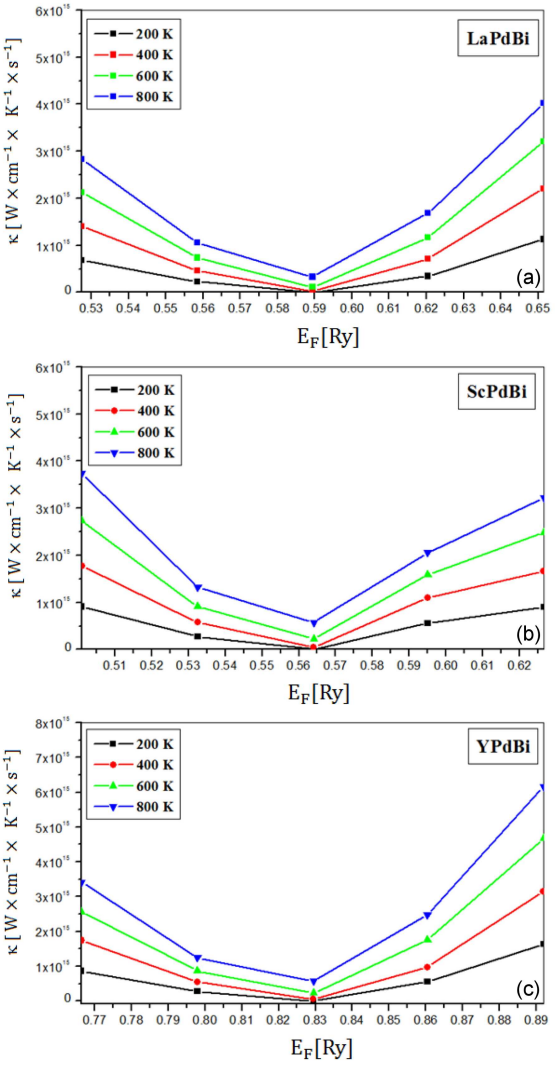

Fig. 14. The variation of the thermal conductivity for XPdBi (X = La (a), Sc (b), Y (c)).

and 3.2006×10^{20} $(\Omega\ \mathrm{m\ s})^{-1}$ obtained for Fermi energies: $E_\mathrm{F} = 0.651$ Ry at T=600 K, $E_\mathrm{F} = 0.626$ Ry at T=200 K, and $E_\mathrm{F} = 0.891$ Ry at T=600 K for the three compounds LaPdBi, ScPdBi, and YPdBi respectively. The thermal conductivities calculated as a function of the Fermi energy are represented in Fig. 14 at different temperatures of 200, 400, 600, and 800 K for the three compounds XPdBi (X = La, Sc, Y). The LaPdBi, ScPdBi, and YPdBi semiconductors are characterized by very low thermal conductivity due to lattice vibrations, which makes them suitable materials for the best applications in thermoelectric devices. The three compounds LaPdBi, ScPdBi, and YPdBi exhibit similar behavior. The value of the thermal conductivity of the three compounds LaPdBi, ScPdBi, and YPdBi decreases progressively until $E_\mathrm{F} = 0.59$ Ry, $E_\mathrm{F} = 0.564$ Ry, and $E_\mathrm{F} = 0.83$ Ry, respectively, then increases beyond these values. It is clear that the thermal conductivity at the temperature of 800 K is greater than that corresponding to 200, 400, and 600 K for the three compounds LaPdBi, ScPdBi, and YPdB. The free electrons in these compounds absorb increasing energy resulting in more heat transfer. The trend of electronic–thermal conductivity is similar to that of electrical conductivity because charge carriers are also heat carriers. Figure 15 shows the variation in the Seebeck coefficient (S) as a function of the Fermi energy at T = 200, 400, 600, and 800 K for the three compounds XPdBi (X = La, Sc, Y). It is clearly seen that the highest value of the Seebeck coefficient (in absolute value) for the three compounds is obtained at the temperature of 200 K. The Seebeck coefficient has the particularity of being positive or negative depending on the nature of the majority charge carriers of the material. If $S < 0$, then the majority of carriers are electrons, and the material is said to be n-type. Conversely, if $S > 0$, then the principal carriers are holes, and the material is said

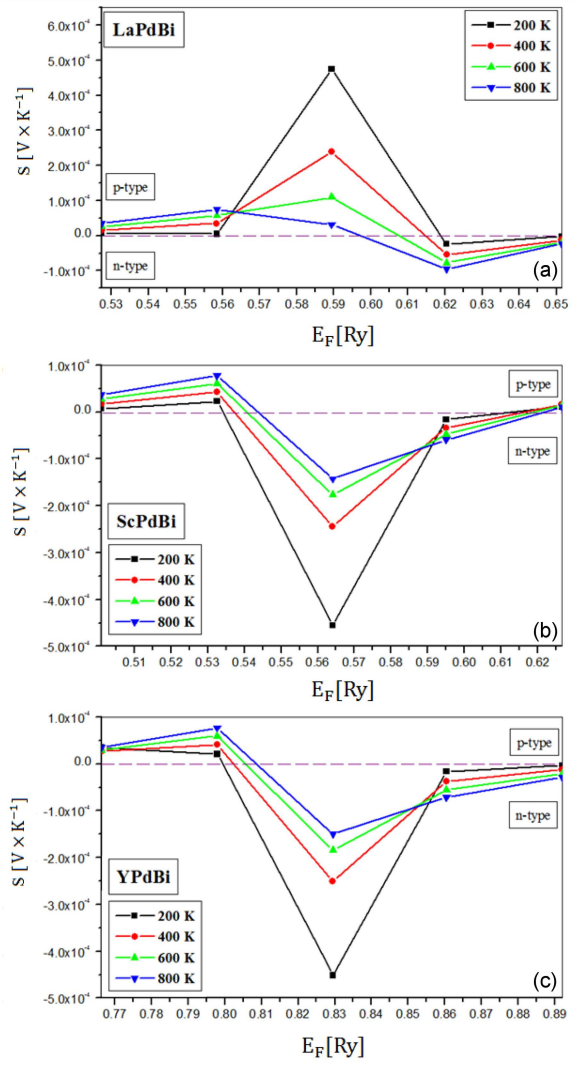

Fig. 15. The variation of the Seebeck Coefficient for XPdBi (X = La (a), Sc (b), Y (c)).

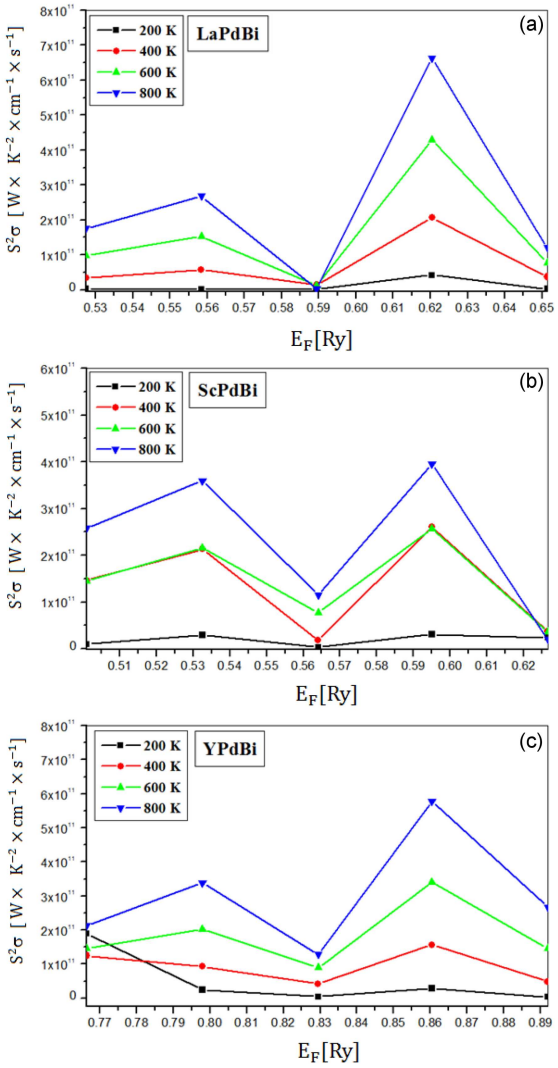

Fig. 16. The variation of the power factor for XPdBi (X = La (a), Sc (b), Y (c)).

to be p-type [33–35]. This effect is the basis for temperature measurement applications that use thermocouples and electricity generation. The Seebeck coefficient has a maximum value of approximately 4.7446×10^{-4} V/K, 4.5131×10^{-4} V/K, and 4.5131×10^{-4} V/K corresponding to the value of 0.59, 0.564, and 0.83 Ry of the Fermi energy at T=200 K for the three compounds LaPdBi, ScPdBi, and YPdBi, respectively. For the compound LaPdBi at T=200 K and $E_F = 0.59$ Ry, the Seebeck coefficient indicates that the electrons are the dominant charge carriers ($S > 0$); therefore, this material is p-type. While the Seebeck coefficient of the ScPdBi and YPdBi compounds at $E_F = 0.564$ Ry and $E_F = 0.83$ Ry, respectively, suggests conduction by holes ($S > 0$) at T=200 K; therefore, they are p-type. Figure 16 shows the power factor as a function of the Fermi energy at T = 200, 400, 600, and 800 K for the three compounds XPdBi (X = La, Sc, Y). It is noted that the power factor at the temperature of 800 K is greater than that at 200, 400, and 600 K for the three compounds LaPdBi, ScPdBi, and YPdB. The power factor had a maximum value of approximately 6.620×10^{11} W/(K^2 cm s), 3.955×10^{11} W/(K^2 cm s), and 5.783×10^{11} W/(K^2 cm s), corresponding to the value of 0.62, 0.595, and 0.86 Ry of the Fermi energy at T=800 K for the three compounds LaPdBi, ScPdBi, and YPdBi, respectively. The power factor of the three materials XPdBi (X = La, Sc, Bi) presents a main peak calculated by mBJ-GGA with a strong intensity on the side of the doping n. The maximum power factor values of the three materials are attributed to their very high electrical conductivities. The figure of merit (ZT) predicts the performance of thermoelectric material and the ability of a given material to efficiently produce thermoelectric power. Materials with ZT close to or greater than unity are good candidates for thermoelectric devices [36, 37]. Our plots of the figure of merit as a function of

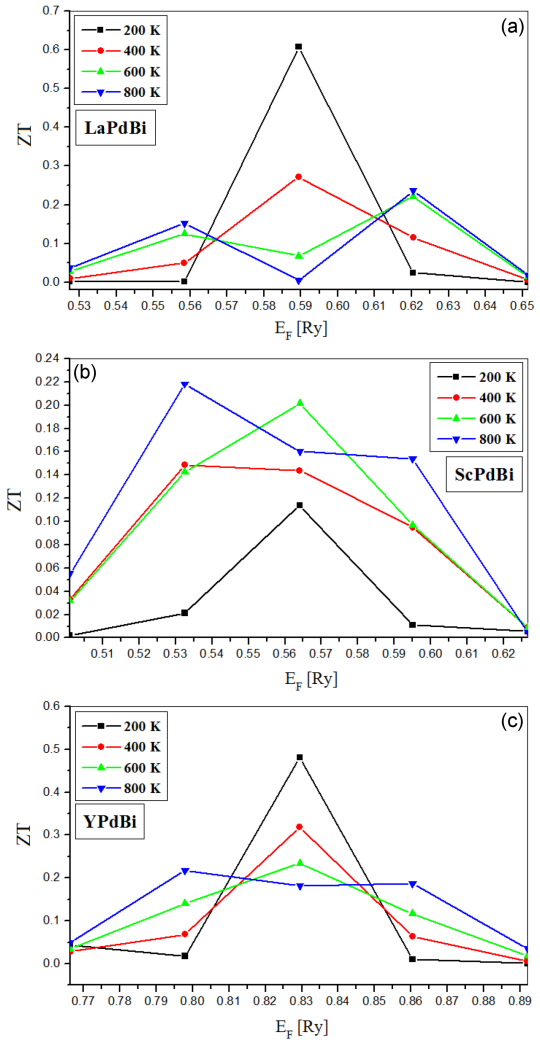

Fig. 17. The variation of the figure of merit (ZT) for XPdBi (X = La (a), Sc (b), Y (c)).

Fermi energy at different temperatures are given in Fig. 17 for the three compounds LaPdBi, ScPdBi, and YPdBi. The figure of merit is given by the following relationship $ZT = \sigma S^2 T/\kappa$ [14] where S is the Seebeck coefficient, σ is the electrical conductivity, T is the temperature, and κ is the thermal conductivity. In Fig. 15, we notice that the ZT behavior of the three compounds LaPdBi, ScPdBi, and YPdBi is different. At temperature 200 K, the maximum values of the ZT are 0.608 and 0.481, obtained at 0.589 Ry and at 0.829 Ry for LaPdBi and YPdBi, respectively, while the maximum value of the ZT of the ScPdBi alloy is 0.218 obtained at 0.532 Ry and at T = 800 K. To our knowledge regarding the thermoelectric properties as a function of the Fermi energy and at T = 200, 400, 600, and 800 K, no study has yet been reported in the literature on the compounds ScPdBi and YPdBi. For the LaPdBi alloy, the Seebeck coefficients, power factor, and thermal conductivity are in good agreement with available experimental data [18, 28].

4. Conclusions

In this work, we investigated the different physical properties of the XPdBi (X = La, Sc, Y) materials using the FP-LAPW method based on density functional theory. For this reason, we are interested in studying the half-Heusler LaPdBi, ScPdBi, and YPdBi alloys due to their technological and industrial applications. The equilibrium lattice parameters and the Bulk modulus are very well reproduced by the GGA-PBE approximation. The equilibrium lattice parameters were found to be in good agreement with those given by the experiments and other theoretical works. The study of electronic band structures shows that the compounds LaPdBi, ScPdBi, and YPdBi have a semiconductor character. The density of states gives a detailed explanation of the contribution of atoms for different orbitals in the electronic structure. The valence band is strongly dominated by the Pd-d states, and the conduction band is dominated by the La-f, Sc-d, and Y-d states. We know that the optical properties of a material are very important from an optoelectronic point of view, so a qualitative study of the real and imaginary dielectric function, the refractive index, the extinction coefficient, the absorption coefficient, reflectivity, and optical conductivity were presented. It is deduced therefrom that the optical properties of the three compounds are comparable. The prediction of the optical properties shows that the studied compounds LaPdBi, ScPdBi, and YPdBi are ideal materials for optoelectronic applications, renewable energies, and solar cells. Finally, using the BoltzTraP code, we studied the thermoelectric properties of LaPdBi, ScPdBi, and YPdBi compounds. Analysis of the dependence Seebeck coefficients on the Fermi energy, power factor, figure of merit, electrical conductivity, and thermal conductivity at different temperatures revealed that the compounds possess attractive characteristics, making them promising materials for future thermoelectric device applications. This comparative and detailed study may encourage new experimental efforts on semi-Heusler thermoelectric materials to find materials with high thermoelectric properties and may contribute to the development of more efficient devices for optoelectronic and thermoelectric applications.

References

[1] Jiangang He, Maximilian Amsler, Yi Xia, Shahab Naghavi, Vinay Hegde, Shiqiang Hao, Stefan Goedecker, Vidvuds Ozoliós, Chris Wolverton, *Phys. Rev. Lett.* **117**, 046602 (2016).

[2] A. Touia, C. Khobzaoui, M. Benkhaled, M. Fodil, *J. Supercond. Nov. Magn.* **34**, 1865 (2021).

[3] A. Ababou, F. Chiker, H. Khachai, R. Miloua, R. Khenata, R. Ahmed, S.H. Naqib, A. Bouhemadou, S. Bin Omran, F. Boukabrine, *Physica B: Condens. Matter* **601**, 412584 (2021).

[4] F. Tran, "WIEN2k: An Augmented Plane Wave Plus Local Orbitals Program for Calculating Crystal Properties", *RaProChe 2018*, Roscoff (France) 2018.

[5] R.M. Shabara, *Mater. Res. Express* **4**, 086511 (2017).

[6] B.A. Cook, J.L. Harringa, *J. Mat. Sci.* **34**, 323 (1998).

[7] H.-L. Zhang, S. Chadov, L. Müchler, B. Yan, X.-L. Qi, J. Kübler, S.C. Zhang, C. Felser, *Phys. Rev. Lett.* **106**, 156402 (2011).

[8] R. Majumder, S.K. Mitro, *RSC Adv.* **10**, 37482 (2020).

[9] I. Karla, J. Pierre, R.V. Skolozdra, *J. Alloys Compd.* **265**, 42 (1998).

[10] Yongchun Gao, Xingang Guo, Jianwei Lu, Int. J. Sci. **2**, (2015).

[11] Xiao Zhang, Li-Dong Zhao, *J. Materiomics* **1**, 92 (2015).

[12] J.P. Perdew, K. Burke, M. Ernzerhof, *Phys. Rev. Lett.* **77**, 3865 (1996).

[13] F. Tran, P. Blaha, *Phys. Rev. Lett.* **102**, 226401 (2009).

[14] A. Touia, K. Benyahia, A. Tekin, *J. Supercond. Nov. Mag.* **34**, 2689 (2021).

[15] F.D. Murnaghan, *Proc. Natl. Acad. Sci.* **30**, 244 (1944).

[16] M.G. Haase, T. Schmidt, C.G. Richter, H. Block, W. Jeitschko, *J. Solid State Chem.* **168**, 18 (2002).

[17] B. Nowak, D. Kaczorowski, *J. Phys. Chem. C* **120**, 21797 (2016).

[18] T. Sekimoto, K. Kurosaki, H. Muta, S. Yamanaka, *MRS Online Proceedings Library* **886**, 804 (2005).

[19] N. Korozlu, K. Colakoglu, E. Deligoz, G. Surucu, *Balkan Phys. Lett.* **18**, 181040, 302 (2010).

[20] Jiong Yang, Huanming Li, Ting Wu, Wenqing Zhang, Lidong Chen, Jihui Yang, *Adv. Funct. Mater.* **18**, 2880 (2008).

[21] S.D. Ramarao, A. Pawbake, A. Kumar Singh, M. Núñez-Regueiro, M.-A. Méasson, S.C. Peter, *J. Alloys Compd.* **848**, 156632 (2020).

[22] Zhipeng Hou, Yue Wang, Enke Liu, Hongwei Zhang, Wenhong Wang, Guangheng Wu, *Appl. Phys. Lett.* **107**, 202103 (2015).

[23] J.-C.G. Bunzli, V.K. Pecharsky, *Handbook on the physics and chemistry of rare earths*, 1st Ed., Elsevier, 2012.

[24] A. Bhattacharya, V. Bhardwaj, B.K. Mani, J.K. Dutt, R. Chatterjee, *Sci. Rep.* **11**, 12029 (2021).

[25] Gangqian Ding, G.Y. Gao, Li Yu, Yun Ni, KaiLun Yao, *J. Appl. Phys.* **119**, 025105 (2016).

[26] M. Narimani, Z. Nourbakhsh, *Modern Phys. Lett.* **30**, 1650159 (2016).

[27] M. Narimani, Z. Nourbakhsh, *Thin Solid Films* **616**, 287 (2016).

[28] T. Sekimoto, K. Kurosaki, H. Muta, S. Yamanaka, *Mater. Trans.* **48**, 2079 (2007).

[29] Junli Zhang, Zhipeng Hou, Chenhui Zhang, Jie Chen, Peng Li, Yan Wen, Qiang Zhang, Wenhong Wang, Xixiang Zhang, *Appl. Phys. Lett.* **115**, 172407 (2019).

[30] N.P. Armitage, arXiv:0908.1126, 2009.

[31] M. El Amine Monir, H. Ullah, H. Baltach, Y. Mouchaal, O. Merabiha, A. Bahnes, D. Rached, *Int. J. Mod. Phys.* **32)**, 1850116 (2018).

[32] A. Touia, K. Benyahia, I.S. Messaoudi, A. Tekin, *Acta Phys. Pol. A* **141**, 210 (2022).

[33] D.W. Rowe, *Handbook of Thermoelectrics CRC Press*, New York 1995, p. 299.

[34] E. Altenkirch, *Phys. Z.* **10**, 560 (1909).

[35] E. Altenkirch, *Phys. Z.* **12**, 920 (1911).

[36] O. Rabina, Yu-Ming Lin, M.S. Dresselhaus, *Appl. Phys. Lett.* **79**, 81 (2001).

[37] T. Takeuchi, *Mater. Trans.* **50**, 2359 (2009).